V. K. Zotta, L. Garzotti, F. J. Casson, D. Frigione, F. Koechl, E. Lerche, P. Lomas, F. Rimini, M. Sertoli, D. Van Eester, R. Gatto, C. Mazzotta, G. Pucella

Fusion power predictions for beta_N = 1.8 baseline scenario in preparation to D-T operations at JET

Fusion power predictions for beta_N = 1.8 baseline scenario in preparation to D-T operations at JET

V. K. Zotta, L. Garzotti, F. J. Casson, D. Frigione, F. Koechl, E. Lerche, P. Lomas, F. Rimini, M. Sertoli, D. Van Eester, R. Gatto, C. Mazzotta, G. Pucella

Fusion power predictions for $\beta_N \approx 1.8$ baseline scenario in preparation to D-T operations at JET

V. K. Zotta[1], **L. Garzotti**[2], **F. J. Casson**[2], **D. Frigione**[3], **F. Köchl**[2], **E. Lerche**[2], **P. Lomas**[2], **F. Rimini**[2], **M. Sertoli**[2], **D. Van Eester**[4], **R. Gatto**[1], **C. Mazzotta**[5], **G. Pucella**[5] and **JET Contributors***

[1]Sapienza University of Rome, Rome, Italy
[2]CCFE, Culham Science Centre, Abingdon, UK
[3]University of Tor Vergata, Rome, Italy
[4]Laboratory for Plasma Physics, LPP-ERK/KMS, Bruxelles BE
[5]ENEA C. R. Frascati, Frascati, Italy
*See the author list of *Overview of JET results for optimising ITER operation* by J. Mailloux et al. to be published in Nuclear Fusion Special issue: Overview and Summary Papers from the 28th Fusion Energy Conference (Nice, France, 10-15 May 2021)

Abstract. The fusion performance of ELMy H-mode DT plasmas with $q_{95} \approx 3$ and $\beta_N \approx 1.8$ (also referred to as medium-β_N baseline scenario in the rest of this paper) are predicted with the JINTRAC suite of codes and the QuaLiKiZ transport model.

The predictions are based on the analysis of plasmas from the first DT campaign on JET in 1997 (DTE1) and pure deuterium plasmas developed at JET in preparation for the DT experimental campaign in 2021 (DTE2), after the installation of a Be/W ITER-like wall (ILW) in 2011.

The sensitivity of the predictions to plasma parameters such as current, toroidal field, pedestal confinement and impurity content are analysed together with the sensitivity to the amount of auxiliary heating power available.

The simulations indicate that a fusion power of 10 MW should be achievable under a fairly wide range of assumptions, provided that the auxiliary heating power is around or above 38 MW. Higher fusion power approaching 15 MW could be achievable for this value of β_N only for particularly pure plasmas and with 40 MW of additional heating power.

1. Introduction

After a first deuterium-tritium (DT) experimental campaign in 1997 (DTE1) the JET tokamak will operate in DT again in 2021 (DTE2). DTE2 will be substantially different from DTE1 because, since DTE1, in subsequent upgrades, JET has had the original C first wall replaced with an ITER-like wall (ILW) made of Be and W, increased its additional heating power and expanded the set of available diagnostics. The focus of DTE2 will be different from DTE1 as the emphasis will be placed on the stationary nature of the performance instead of the record peak fusion power. The DTE2 target performance is 15 MW of fusion power averaged for 5 s [1].

In preparation to DTE2, experiments have been performed on JET to prepare the plasma scenarios in D, which will be used in DTE2 [2, 3, 4]. Two scenarios are being developed: the baseline scenario where the confinement is achieved at high plasma current ($I_p \geq 3.5$ MA) and medium normalized beta (≈ 1.8), and the hybrid scenario, which relies on a lower plasma current ($I_p \leq 2.5$ MA) a higher normalized beta (2-3) to achieve good confinement.

These plasmas have been the object of an intense activity of modelling in order to extrapolate the performance from D to DT and quantify the uncertainty affecting the predicted results [5, 6]. In this paper we concentrate on the baseline scenario and we use the transport model QuaLiKiZ to predict the DT performance of typical baseline plasmas under a variety of assumptions.

Although some of the best performing baseline plasmas are characterized by a normalized beta β_N=2.2 they might be not extrapolable at plasma currents higher than 3.8 MA due to the limited additional heating power available on JET. Therefore, in this paper we concentrate on medium β_N (≈ 1.8) baseline plasmas as a basis for our extrapolation.

The paper is structured as follows. In section 2 we describe the modelling assumptions and the result of our modelling of a medium β_N plasma obtained on JET with the ILW. In section 3 we test the extrapolability to DT plasmas of the simulations described in the previous section by modelling two baseline-like ELMy H-mode plasmas (one in D and one in DT) from DTE1. In section 4 we extrapolate the performance of the reference discharge to DT in presence of an ILW and we investigate the effect of modifying some of the modelling assumptions. In section 5 we discuss the results and in section 6 we give conclusions of our study.

2. Modelling the reference discharge

The baseline plasma used as reference for the modelling and the extrapolations presented in this paper is JET pulse 92376 ($\beta_N \approx 1.8$). This is an H-mode plasma with B_T=2.8 T, I_p=3 MA and 26 MW of additional heating power, 22 MW from neutral beam injection (NBI), and 4.4 MW from ion cyclotron resonance heating (ICRH) in H minority heating scheme.

The time traces of the relevant plasma parameters are shown in the figure 1 and the main plasma parameters averaged over the time window of interest (between 9.6 s and 10.7 s) are reported in table 1.

The modelling of this plasma has been performed with the JINTRAC suite of codes [7] using the QuaLiKiZ first-principle transport model [8, 11]. Note that QuaLiKiZ takes into account some possible linear isotope effects on the main ion transport, but does not capture other non-linear effects at high β [9, 10]. However, given the moderate β of the plasmas used in this paper as a basis for the extrapolation, these non-linear effect are not crucial and therefore QuaLiKiZ can be considered suitable for the extrapolation to DT plasmas.

The simulations are performed in a fully predictive way. In particular, we model the evolution of plasma current density, ion density, electron and ion temperature and plasma rotation. In addition the evolution of the density of a number of impurities was modelled by the impurity transport code SANCO [12]. The impurity transport model includes neo-classical transport from NCLASS [13] and anomalous transport provided by QuaLiKiZ.

The initial conditions for the electron density and temperature profiles were taken from the measurements of the JET high resolution Thomson scattering system (HRTS) [14] and for the ion temperature and plasma toroidal rotation from beam charge exchange spectroscopy (CX) [15].

In this simulation an impurity mix of Be, Ni and W was considered and the relative concentration of the impurity species were prescribed according to an estimate taking into account several diagnostics and described in [16].

The boundary conditions are imposed at the separatrix and the heat transport in the edge transport barrier (ETB) is adjusted in order to match the experimental height of the temperature pedestal. The width of the pedestal is imposed to match the experimental value. Once the heat transport in the ETB has been fixed we assumed a χ/D ratio in the pedestal of 4 and tuned the wall recycling particle source to match the density at the top of the ETB.

The heat sources were modelled by means of the PENCIL [17] and PION [18] codes for the NBI and ICRH heating source respectively. The synergy between NBI and ICRH is taken into account self-consistently in JINTRAC (see, for example, [19]). It should be noted that the collisional heating of the electrons by the alpha particles produced by fusion reactions is self-consistently taken into account in the modelling. However, the alpha particle concentration is ignored in the PION calculation of the ICRH absorption. Separate estimates of the role played by the alpha particle as an ICRH absorber indicate that this should be negligible in the scenario considered in this paper.

The equilibrium was computed self-consistently with the evolution of the current and kinetic profiles by means of the ESCO equilibrium solver [20].

The simulation results for the reference pulse are shown in figures 2, where we show the electron density and electron and ion temperature profiles compared to the experimental measurements and in figures 3, where we show the modelled neutron rate,

Z_{eff} and radiated power compared to the experimental values.

It can be seen that the general agreement between simulation and experiment is good. In particular there is very good agreement between the experimental and modelled kinetic profiles (electron density, electron and ion temperature) and the measured and modelled radiated power. Z_{eff} is underestimated throughout the simulation windows and the measured neutron rate is initially underestimated by about 30-40% but the predicted value approaches the experimental one from half way through the simulation to the end of the modelled time window.

Moreover, the pedestal pressure calculated in our simulation is 8.5 MPa, very close to the experimental one of 8.8 MPa. This is shown in figure 4 showing the resulting pedestal pressure from a scan of electron and ion thermal diffusivities in the pedestal (including $\chi_e = \chi_i = 0.75$ m^2/s, the value chosen for this simulation) and indicating that not only the first-principle transport model captures the details of the reference plasma core, but also that the empirical modelling of the pedestal can be considered realistic.

To further validate the modelling of an ILW baseline plasma, based on the simulations parameter used for shot 92376, we produced a blind prediction of JET shot 96482, a 3.5 MA, 3.35 T plasma. The evolution of the main plasma parameters for shot 96482 is shown in figure 5 and the values of the most relevant plasma quantities averaged of the the time window targeted by the blind simulation are shown in table 1.

The blind simulation was obtained by scaling the initial density from shot 92376 at constant Greenwald fraction and imposing the nominal additional heating power for shot 96482, but leaving the remaining simulation parameters (including the tarnsport coefficients in the pedestal) unchanged. The results are shown in figure 6 and 7, where we show the same plasma parameters as for shot 92376 compared with the experimental ones.

As it can be seen this simulations does an excellent job at predicting the higher current discharge and an even better match with the experiment can be obtained by tuning the the ionization source and using the correct impurity mix for the higher current shot.

3. Modelling DTE1 plasmas

To extend the validation of the model to be deployed for the prediction of performance in DTE2 to a DT plasma we simulated two ELMy H-mode discharges from DTE1. The pulses considered are JET pulses 42464 and 42982. Both plasmas have $I_p = 3.8$ MA, $B_T = 3.8$ T, a C plasma facing wall (and, consequently a different impurity mix with respect to the references modelled in the previous section) and use a ^{3}He minority ICRH heating scheme (as opposed to the H minority scheme used in the shots described in the previous section). Shot 42464 is a pure deuterium plasma, whereas shot 42982 is a 50-50 DT plasma.

The evolution of the plasma parameters for these two plasmas is shown in figures

8 and 9, whereas the average values over the time window of interest are reported in table 1. Further details on these shots can be found in [21] and interpretative transport analysis, in the context of a wider study of ELMy H-mode DT plasmas on JET, can be found in [22].

The same modelling procedure described in the previous section is applied and the comparison between experiment and simulation results are shown in figure 10 and 11 for shot 42464 and 12 and 13 for shot 42982.

The agreement between experiment and simulation in generally good, except for a tendency of QuaLiKiZ to overestimate the peaking of the electron density profiles. The cause of this discrepancy is not clear. A possible reason could be the fairly strong sensitivity of the main ion density profile peaking predicted by QuaLiKiZ to the details of the profiles of quantities such as the safety factor q, the plasma rotation and the impurity density and to the fact the the simulation does not match exactly these plasma paratmeters.

A detailed investigation of the sensitivity of the density peaking to QuaLiKiZ input parameters is beyond the scope of this paper and, given that the overprediction of the density peaking significantly affects only a relatively small volume of plasma ($\psi_N \leq 0.2 - 0.3$) we considered the agreement sufficient to proceed with the extrapolations to DTE2.

4. Extrapolation to DTE2

In order to extrapolate the modelling described in the previous sections to the DT plasmas to be produced in DTE2, we started from the reference simulations of shot 92376 and increased the current and the magnetic field in three steps to 3.8 MA, 4.2 MA and 4.5 MA, increasing the density in order to keep the Greenwald fraction constant, making the optimistic assumption of 40 MW of additional power (34 MW from NBI and 6 MW from ICRH, see [2]) and fixing the field at 3.7 T. The limit on the field was imposed by the duration of the flat top necessary to achieve a 5 s window of optimized performance and by I^2t limits on the JET toroidal field coils. This means that the extrapolation are not done at constant q_{95}, but q_{95} varies from 3 at 3.8 MA to 2.7 at 4.5 MA.

In extrapolating the pedestal parameters to higher current we scaled the target density at the top of the pedestal with the current in order to keep the Greenwald fraction costant and assumed the same pedestal width, particle and heat transport as in the reference case.

In order to take into account a certain degree of uncertainty linked to the expected pedestal performance we repeated the simulations and increased/decreased the electron and ion thermal conductivity in the ETB by 25%.

The effect of the uncertainty in the impurity mix was quantified by performing simulations assuming Ni and Be as dominant impurity and keeping Z_{eff} constant. A third series of simulations was performed including W in the impurity mix to improve the

modelling of the radiated power and to maintain the ratio P_{rad}/P_{aux} constant throughout the simulations.

The results of this first series of runs are plotted in figure 14 where we show the expected fusion power for the different cases. The error bars represent the effect of the uncertainty in the pedestal transport. It can be seen that the fusion power does not increase significantly with plasma current above 3.8 MA and even decreases slightly if W is included in the impurity mix. This is due partly to the fact that the additional power is kept constant rather than increased proportionally to the density, leading to a progressive reduction of the ion temperature in the core, and partly to the fact that, with increased density, the NBI penetration is shallower, resulting in a lower heating source in the plasma core.

The NBI deposition profiles for the three plasma currents considered in this study are shown in figure 15 where we plot the NBI particle source, ion and electron heat deposition and driven current.

As for the effect of the impurity mix, it can be seen that assuming that Z_{eff} comes entirely from Be introduces a significant plasma dilution and the maximum fusion power achievable in this case is 10 MW. The assumption of a more realistic impurity mix of Be, Ni and W based on an empirical estimate of the relative concentration of these species for the reference shot 92736 does not change dramatically the result with respect to the case with Ni only.

Finally we investigated the effect of the available additional power on the performance and we gradually reduced it from 40 MW to 38 MW (32 MW from NBI and 6 MW of ICRH), 36 MW (32 MW form NBI and 4 MW of ICRH) and 33 MW (29MW of NBI and 4 MW of ICRH) respectively. The results are shown in figure 16 where we plot the different scans for different plasma currents and show that to approach 10 MW of fusion power at least 38 MW of additional heating power will be needed.

5. Discussion

The simulations presented in this paper predict the fusion power in baseline scenario at medium β_N (≈ 1.8)in DTE2. As stated in the introduction, the interest in these plasmas is due the fact that they are more easily extrapolable to higher field and current and more representative of a typical baseline scenario than the higher β_N, peak performance plasmas considered in the past.

The transport model used in the extrapolation is the QuaLiKiZ model, which reproduces well pure D plasmas produced in JET with an ILW and is in reasonable agreement with plasmas from DTE1 (JET with C wall) apart for the overprediction of the peaking of the density profile.

The results indicate that, in general, it should be possible to achieve 10 MW of fusion power over 5 s in a fairly wide range of circumstances, provided that 38 MW heating power is available.

Moreover, they suggest that pushing for high current is not necessarily a way

to continuously improve the fusion performance as the increase in density at fixed additional heating power is likely to offset the expected increase in confinement associated with higher current.

The effect of the uncertainties in the pedestal confinement have also being investigated and can be responsible for a variation of about 1 MW of fusion power in excess of defect of the reference case where the pedestal transport was tuned to match the experimental parameters in the reference case at 3 MA. The analysis of the sensitivity to pedestal condition has been motivated by the necessity of taking into account on one side a possible improved pedestal confinement in DT with respect to D and on the other hand by the possibility that the fuelling rate in DT will have to be increased with respect to pure D plasmas to promote the ELMs, which could be less frequent in DT, and are necessary to flush impurities for the plasma edge.

A final analysis has been conducted to investigate the sensitivity to the available additional input power. In order to estimate the effect of different levels heating power we have run simulations for each current level assuming an additional heating power availability of 33 MW (29 MW of NBI and 4 MW of ICRH), 36 MW (32 MW of NBI and 4 MW of ICRH), 38 MW (32 MW of NBI and 6 MW of ICRH) and 40 MW (34 MW of NBI and 6 MW of ICRH). The assumption for the impurity mix was the most realistic one including Be, Ni and W.

This scan shows that the heating power is probably the most critical parameter in determining the highest fusion power achievable and that at least 38 MW of additional heating power will be needed to achieve $P_{fus} = 10$ MW.

In all the cases analyzed the contribution to the total neutron yield was $\approx 60\%$ from thermal reaction and $\approx 40\%$ from beam-target reactions (beam-beam reactions being negligible).

For these medium β_N plasmas, 15 MW of fusion power are achieved only in the best case scenario where the dilution due to Be is minimised, the pedestal confinement is optimized and 40 MW of additional power are injected into the plasma.

6. Conclusions

In this paper we have presented the predictions of the fusion power performance in DTE2 performed using the QuaLiKiZ transport model validated on previous pure deuterium baseline plasmas obtained on JET with ILW and in DT plasmas from DTE1.

Unlike previous result based on the highest performing baseline plasmas with $\beta_N \approx 2.2$, which would be difficult to extrapolate to high field and current due to the limited amount of heating power available on JET heating power, these predictions are based on the baseline scenario at a medium $\beta_N \approx 1.8$.

Results indicate that these plasma can achieve ≈ 10 MW of fusion power at 3.6 MA, 3.7 T and with an additional heating power of at least 38 MW.

Sensitivity analysis indicate that increasing the plasma current further would probably not enhance the performance due to the increase in density at constant heating

power offsetting the positive effect on the confinement of the high current.

The performance is sensitive to the purity of the plasma, the impurity mix to be expected and, ultimately the dilution.

The performance is also extremely sensitive to the amount of heating power available and the indication are that, at this β_N the target value of 15 MW for 5 second can only be achieved in a highly pure plasma and for additional heating power close to 40 MW.

Acknowledgments

References

[1] Joffrin E. *et al* 2019 *Nucl. Fusion* **59** 112021
[2] Garzotti L. *et al* 2019 *Nucl. Fusion* **59** 076037
[3] Mailloux J. *et al* 2021 submitted to *Nucl. Fusion*
[4] Garcia J. *et al* 2021 *Proc. 28th IAEA Fusion Energy Conference* paper EX/1
[5] Garcia J. *et al* 2019 *Nucl. Fusion* **59** 086047
[6] Casson F. J. *et al* 2020 *Nucl. Fusion* **60** 066029
[7] Romanelli M. *et al* 2014 *Plasma and Fusion Research* **9** 3403023
[8] Bourdelle C. *et al* 2016 *Plasma Phys. Control. Fusion* **58** 014036
[9] Garcia J. *et al* 2017 *Nucl. Fusion* **57** 014007
[10] Mariani A. *et al* 2021 Nucl. Fusion **61** 066032
[11] Citrin J. *et al* 2017 *Plasma Phys. Control. Fusion* **59** 064010
[12] Lauro Taroni L. 1994 *Proc. 21st EPS Conference on Controlled Fusion and Plasma Physics* ECA
        vol. **18B**, part I, p. 102
[13] Houlberg W A, Shaing K C, Hirshman S P, Zarnstorff M C, 1997 *Phys. Plasmas* **4** 3230
[14] Pasqualotto R. *et al* 2004 *Rev. Sci. Intrum.* **75** 3891
[15] Hawkes N. C. *et al* 2018 *Rev. Sci. Intrum.* **89** 10D113
[16] Sertoli M. *et al* 2019 *J. Plasma Phys.* **85** 905850504
[17] Challis C. D. *et al* 1989 *Nucl. Fusion* **29** 563
[18] Eriksson L.-G., Hellsten T. and Willén U. 1993 *Nucl. Fusion* **33** 1037
[19] Gallart D. *et al* 2018 *Nucl. Fusion* **58** 106037
[20] Cenacchi G. and Rulli M. 1988 *Upgrading of an equilibrium transport code for a multispecies free-
        boundary plasma*, ENEA Report RTI/TIB(88)5
[21] Horton L. D. *et al* 1999 *Nucl. Fusion* **39** 993
[22] Hyun-Tae Kim *et al* 2020 *Nucl.Fusion* **60** 066003

Table 1. Main plasma parameters for the JET plasmas used as references for the extrapolations presented in the paper.

Shot number	92376	96482	42464	42982
B_T [T]	2.8	3.35	3.8	3.8
I_p [MA]	3.0	3.5	3.8	3.8
q_{95}	3.2	3.2	3.5	3.5
β_N [%/MA]	1.8	1.9	1.2	1.45
P_{NBI} [MW]	22	29	18	21.6
P_{ICRH} [MW]	4.4	4.3	0.5	2.0
n_{e0} [10^{19} m^{-3}]	7.8	9.4	8.5	7.8
$< n_e >$ [10^{19} m^{-3}]	5.8	6.1	5.6	5.8
T_{e0} [keV]	5.4	6.0	7.5	5.8
$< T_e >$ [keV]	2.8	2.5	4.5	3.3
T_{i0} [keV]	6.9	8.0	7.6	10.3
$< T_i >$ [keV]	3.0	3.8	3.7	4.9
W_{th} [MJ]	7.5	10.0	8.3	7.9
Neutron rate [10^{16} [n/s]	1.65	3.0	1.33	168.8
Z_{eff}	1.9	1.8	2.3	2.8
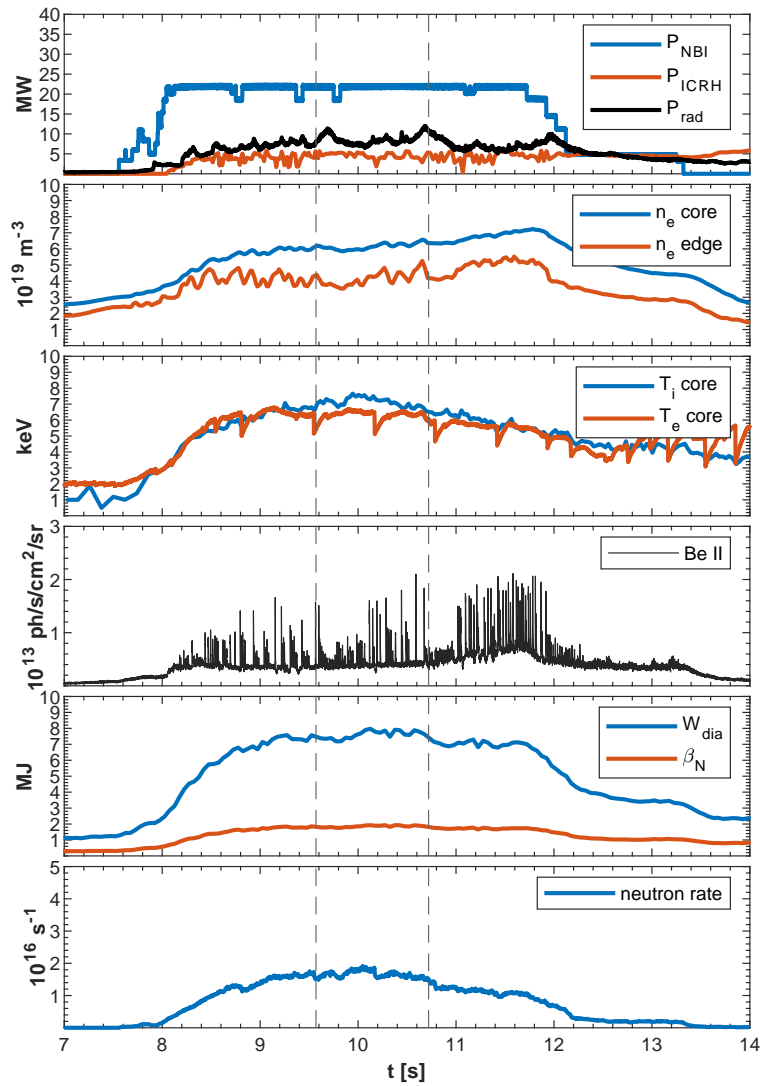
Figure 1. Evolution of main plasma parameters for JET shot 92376, a medium β_N ($\beta_N \approx 1.8$) plasma chosen as reference for the extrapolations presented in this paper. From top to bottom are shown: NBI and ICRH auxiliary heating power and radiated power (from bolometer); core and edge line average electron density (from JET multi-channel infrared interferometer, core electron temperature (from electron cyclotron emission radiometer) and core ion temperature (from high resolution X-ray crystal spectrometer); BeII emission (from visible spectroscopy, showing the ELM behaviour); plasma thermal energy and β_N and neutron rate.
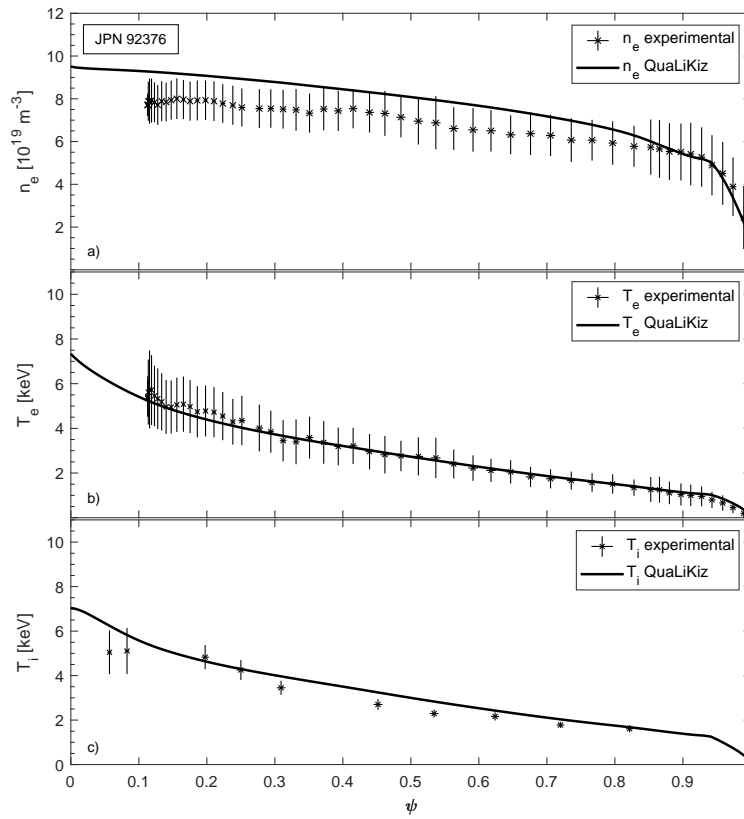
Figure 2. Comparison between experimental and modelled electron density profiles (a), electron temperature profiles (b) and ion temperature profiles (c) for JET shot 92376. The electron density and electron temperature experimental points are Thomson scattering measurements and the ion temperature experimental point are beam charge exchange spectroscopy measurements. All measurements are averaged over the modelled interval (from 9.6 s to 10.7 s) and the vertical error bars combine the RMS over the interval considered and the measurement uncertainty. The horizontal error bar are the RMS of the ψ coordinate mapped from a EFIT equilibrium. The modelled profile is the converged solution after full relaxation of the kinetic profiles.
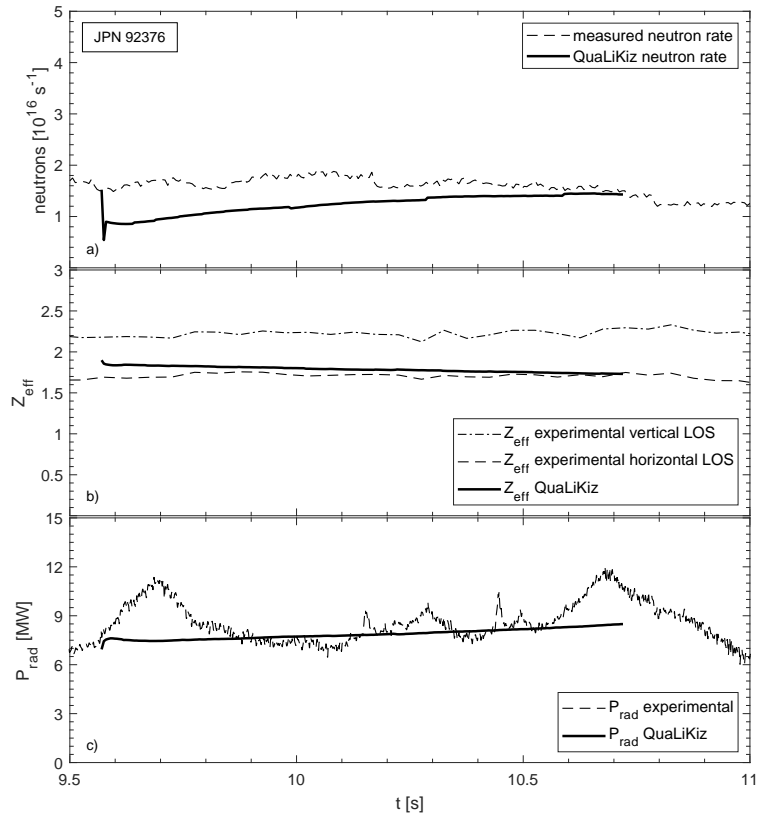
Figure 3. Comparison between experimental and modelled neutron rate (a), Z_{eff} (b) and radiated power (c) for shot 92376. $Z_{e}ff$ is inferred from Brehmsstrahlung measurements along a vertical and a horizontal line of sight across the plasma and radiated power from bolometry.
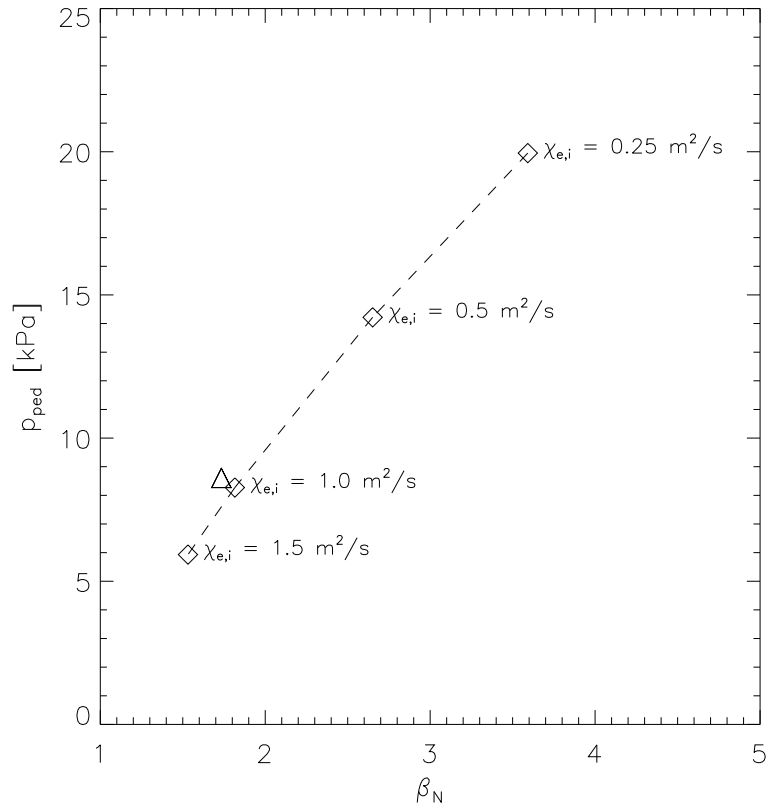
Figure 4. Pedestal pressure as function of β_N obtained in a series of transport simulations of JET shot 92376 where the electron and ion thermal conductivity in the edge transport barrier, $\chi_{e,i}$ was varied by keeping fixed the density at the top of the pedestal (open diamonds). It can be seen that $\chi_{e,i} = 1.0$ m^{2}s-1 gives the best agreement with the experimental point (open triangle).
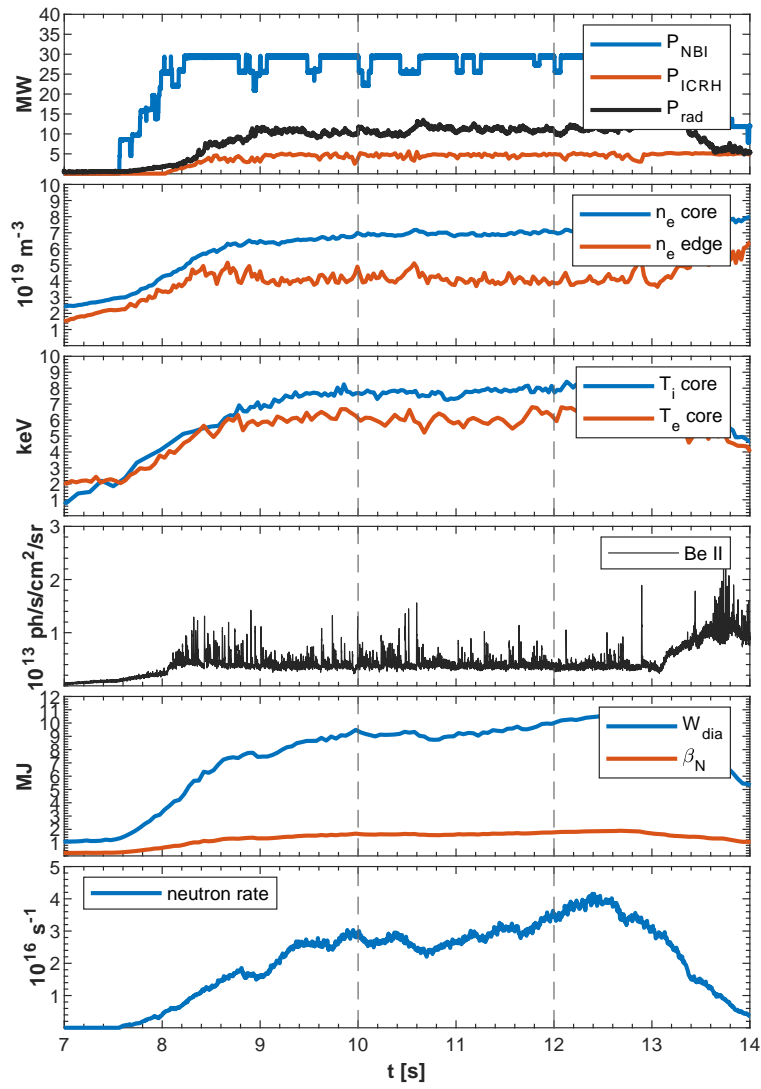
Figure 5. Evolution of main plasma parameters for JET shot 96482, a medium β_N ($\beta_N \approx 1.8$) plasma chosen as target to validate the model tuned on JET shot 92376 and used for the extrapolations presented in this paper. From top to bottom are shown: NBI and ICRH auxiliary heating power and radiated power (from bolometer); core and edge line average electron density (from JET multi-channel infrared interferometer, core electron temperature (from electron cyclotron emission radiometer) and core ion temperature (from high resolution X-ray crystal spectrometer); BeII emission (from visible spectroscopy, showing the ELM behaviour); plasma thermal energy and β_N and neutron rate.
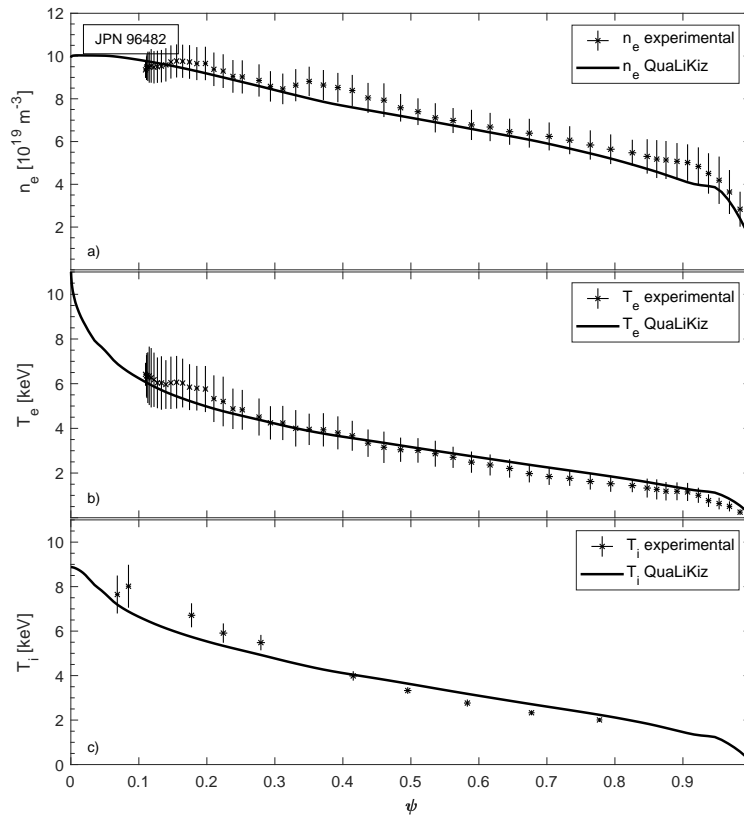
Figure 6. Comparison between experimental and modelled electron density profiles (a), electron temperature profiles (b) and ion temperature profiles (c) for JET shot 96482. The electron density and electron temperature experimental points are Thomson scattering measurements and the ion temperature experimental point are beam charge exchange spectroscopy measurements. All measurements are averaged over the modelled interval (from 9.6 s to 10.7 s) and the vertical error bars combine the RMS over the interval considered and the measurement uncertainty. The horizontal error bar are the RMS of the ψ coordinate mapped from a EFIT equilibrium. The modelled profile is the converged solution after full relaxation of the kinetic profiles.
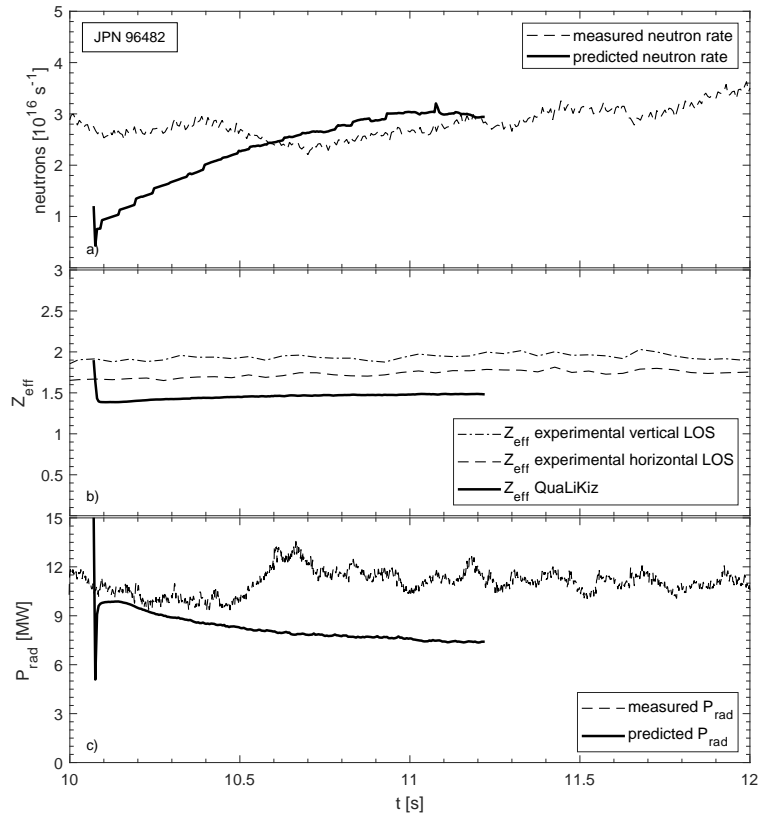
Figure 7. Comparison between experimental and modelled neutron rate (a), Z_{eff} (b) and radiated power (c) for shot 96482. $Z_{e}ff$ is inferred from Brehmsstrahlung measurements along a vertical and a horizontal line of sight across the plasma and radiated power from bolometry.
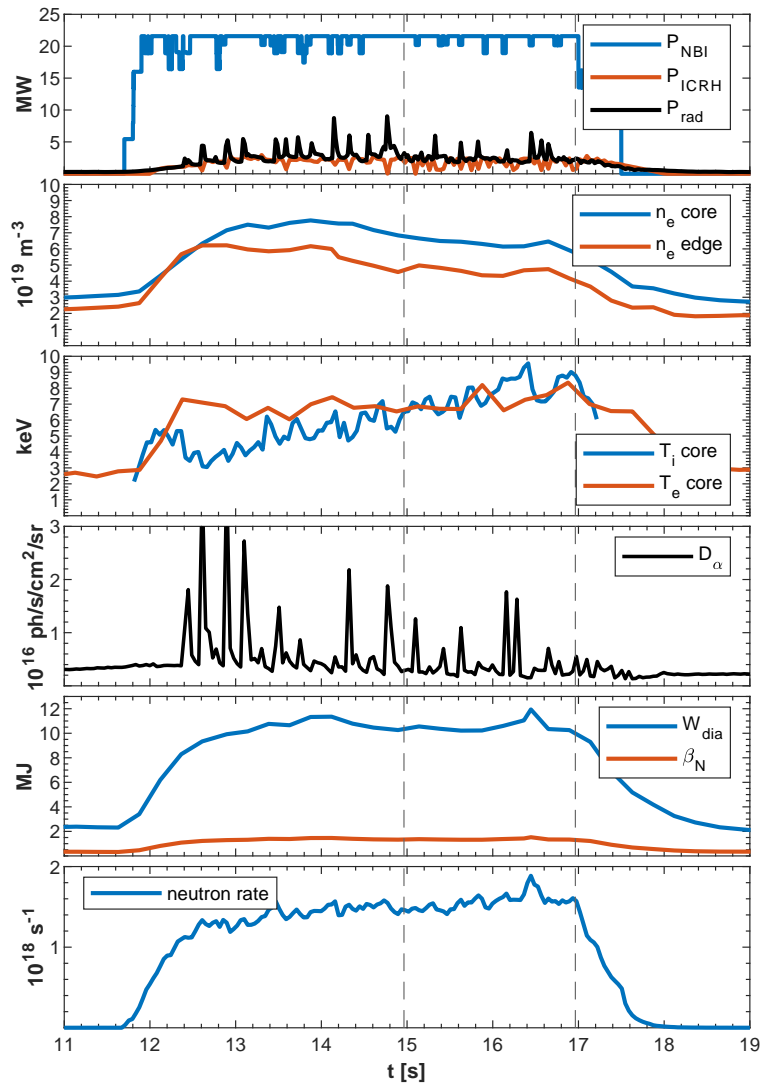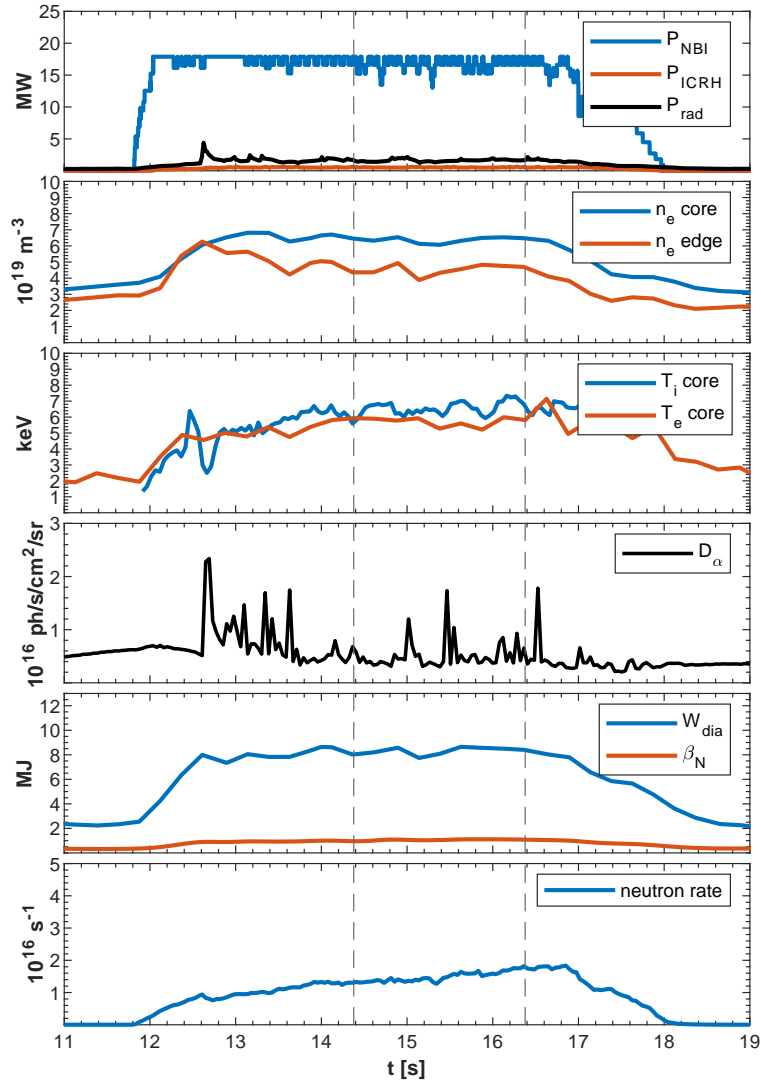
Figure 8. Evolution of main plasma parameters for JET shot 42982, a 50-50 D-T plasma from JET campaign DTE1 chosen as target to validate the model tuned on JET shot 92376 and used for the extrapolations presented in this paper. From top to bottom are shown: NBI and ICRH auxiliary heating power and radiated power (from bolometer); core and edge line average electron density (from JET multi-channel infrared interferometer, core electron temperature (from electron cyclotron emission radiometer) and core ion temperature (from high resolution X-ray crystal spectrometer); BeII emission (from visible spectroscopy, showing the ELM behaviour); plasma thermal energy and β_N and neutron rate.

Figure 9. Evolution of main plasma parameters for JET shot 42464, a pure D plasma from JET campaign DTE1 chosen as target to validate the model tuned on JET shot 92376 and used for the extrapolations presented in this paper. From top to bottom are shown: NBI and ICRH auxiliary heating power and radiated power (from bolometer); core and edge line average electron density (from JET multi-channel infrared interferometer, core electron temperature (from electron cyclotron emission radiometer) and core ion temperature (from high resolution X-ray crystal spectrometer); BeII emission (from visible spectroscopy, showing the ELM behaviour); plasma thermal energy and β_N and neutron rate.
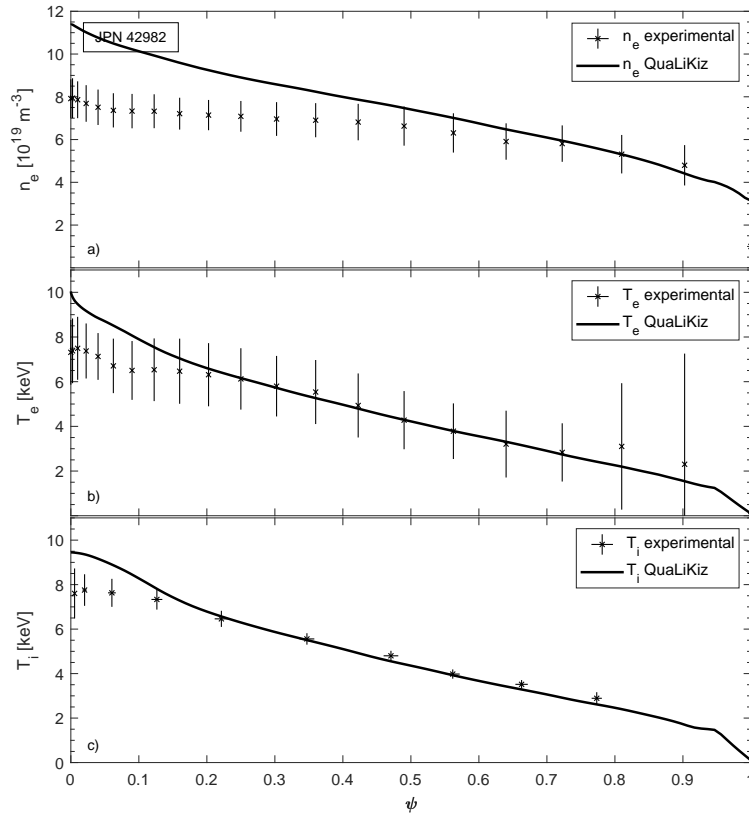
Figure 10. Comparison between experimental and modelled electron density profiles (a), electron temperature profiles (b) and ion temperature profiles (c) for JET shot 42982. The electron density and electron temperature experimental points are Thomson scattering measurements and the ion temperature experimental point are beam charge exchange spectroscopy measurements. All measurements are averaged over the modelled interval (from 9.6 s to 10.7 s) and the vertical error bars combine the RMS over the interval considered and the measurement uncertainty. The horizontal error bar are the RMS of the ψ coordinate mapped from a EFIT equilibrium. The modelled profile is the converged solution after full relaxation of the kinetic profiles.
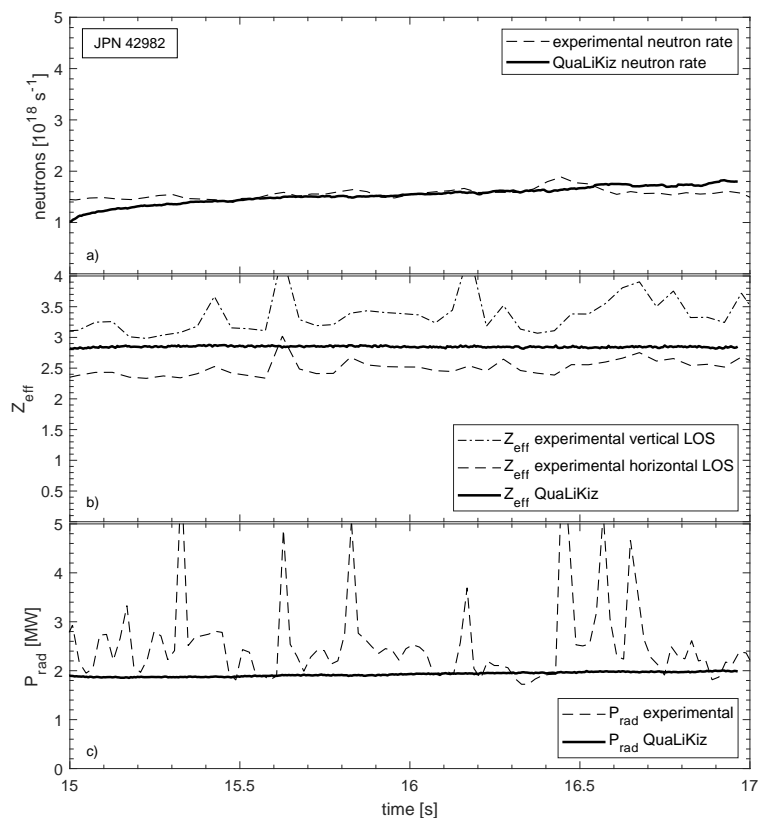
Figure 11. Comparison between experimental and modelled neutron rate (a), Z_{eff} (b) and radiated power (c) for shot 42982. Z_{eff} is inferred from Brehmsstrahlung measurements along a vertical and a horizontal line of sight across the plasma and radiated power from bolometry.
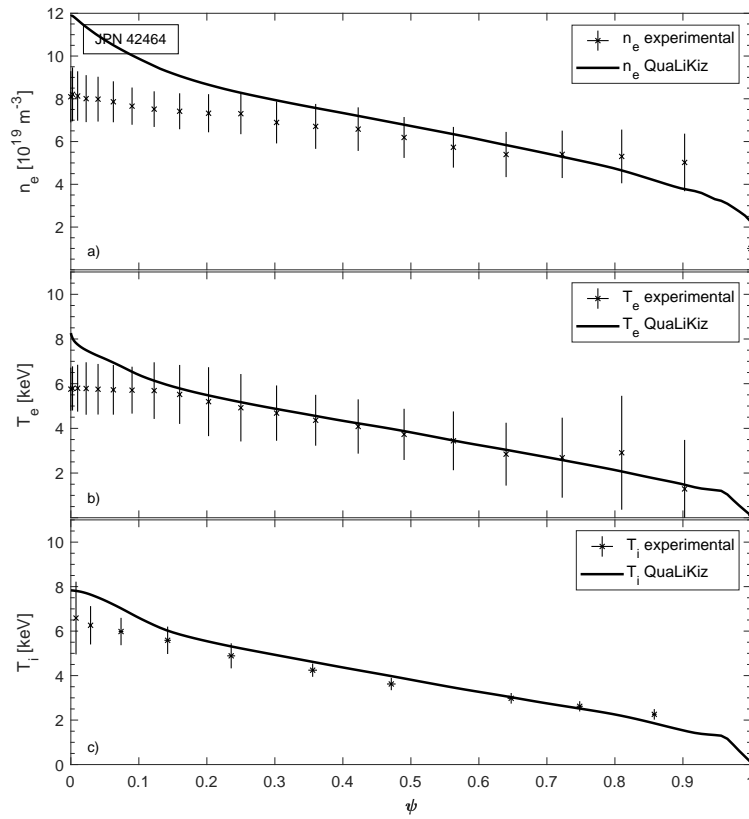
Figure 12. Comparison between experimental and modelled electron density profiles (a), electron temperature profiles (b) and ion temperature profiles (c) for JET shot 42464. The electron density and electron temperature experimental points are Thomson scattering measurements and the ion temperature experimental point are beam charge exchange spectroscopy measurements. All measurements are averaged over the modelled interval (from 9.6 s to 10.7 s) and the vertical error bars combine the RMS over the interval considered and the measurement uncertainty. The horizontal error bar are the RMS of the ψ coordinate mapped from a EFIT equilibrium. The modelled profile is the converged solution after full relaxation of the kinetic profiles.
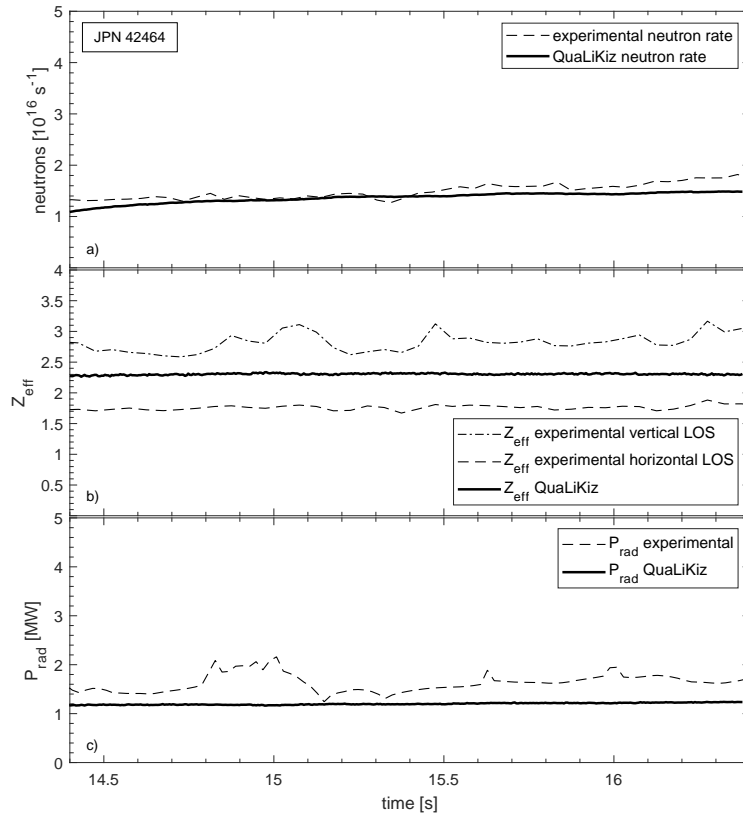
Figure 13. Comparison between experimental and modelled neutron rate (a), Z_{eff} (b) and radiated power (c) for shot 42464. Z_eff is inferred from Brehmsstrahlung measurements along a vertical and a horizontal line of sight across the plasma and radiated power from bolometry.
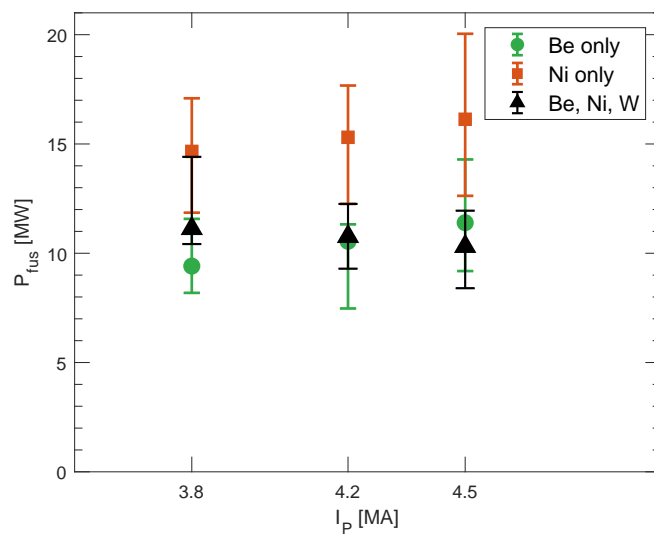
Figure 14. Expected fusion power as function of plasma current and for different impurity mixes for a medium $\beta_N \approx 1.8$ baseline plasma based on shot 92376 assuming 40 MW of additional heating power (32 MW of NBI and 8 MW of ICRH). The error bars correspond to different assumptions on the thermal conductivity in the pedestal.
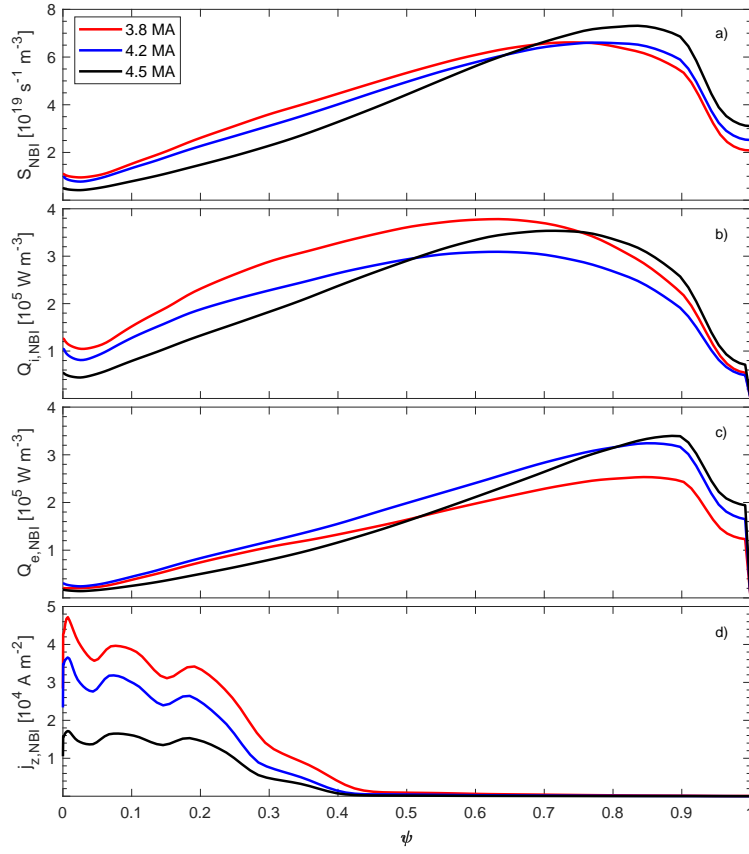
Figure 15. NBI deposition profiles for three different plasma currents and fixed Greenwald fraction. From top to bottom: particle source, ion heat deposition, electron heat deposition and driven current. In all cases the total NBI injected power was 34 MW.
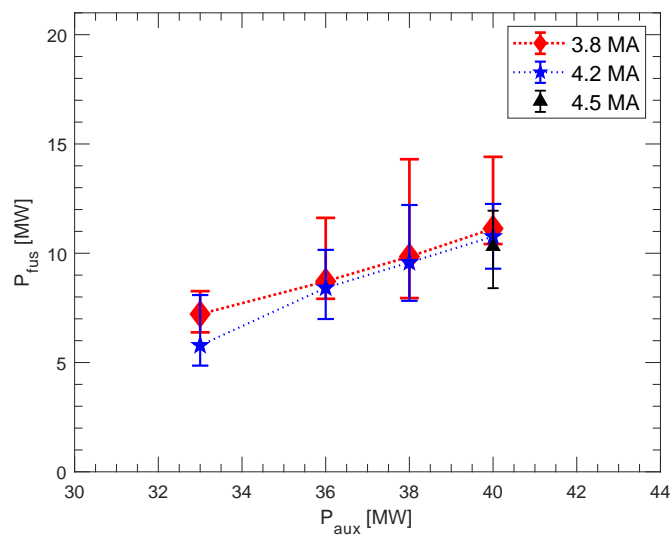
Figure 16. Expected fusion power as function of available heating power for different plasma currents for a medium $\beta_N \approx 1.8$ baseline plasma based on shot 92376 assuming an impurity mix of Be, Ni and W. The error bars correspond to different assumptions on the thermal conductivity in the pedestal.